Progress In Electromagnetics Research, Vol. 119, 191–206, 2011

SUPERRESOLUTION ENHANCEMENT FOR THE SUPERLENS WITH ANTI-REFLECTION AND PHASE CONTROL COATINGS VIA SURFACE PLASMONS MODES OF FINITE THICKNESS ASYMMETRIC STRUCTURE

P.-F. Cao, X.-P. Zhang*, W.-J. Kong, L. Cheng, and H. Zhang

School of Information Science and Engineering, Lanzhou University, Lanzhou 730000, China

Abstract—The paper discusses the reason why the image resolution can be significantly enhanced by the superlens with anti-reflection and phase control coatings (ARPC-superlens) via analyzing the surface plasmons (SPs) modes. ARPC-superlens is an asymmetric structure with finite thickness, in which we first find that there are two asymmetric SPs modes. By comparing the dispersion curve of SPs of ARPC-superlens and the SPs group velocity with their counterparts in the metric ones, we find that the Up Asymmetric Mode and Down Asymmetric Mode are excited within the ARPC-superlens with asymmetric structure. By simulating the aerial images in different SPs modes, the paper also discusses the optimal ratio between the metal slab and the ARPC coatings thickness. The results demonstrate that the subwavelength resolution of ARPC-superlens in Down Asymmetric Mode has been enhanced, when the metal/ARPC thickness ratio is 2:1.

1. INTRODUCTION

A superlens [1] is a slab of negative index material (NIM) [2–4] that can be used to restore the phase of propagating waves and the amplitude of evanescent waves to achieve super-resolution image with lossless media. So far, many approaches of super-resolution imaging with metallic superlens have been reported [5–10]. The metallic superlens is composed of a metal slab and two semi-infinite dielectric

Received 30 May 2011, Accepted 18 July 2011, Scheduled 27 July 2011

* Corresponding author: Xiao-Ping Zhang (zxp@lzu.edu.cn).

media with the same permittivities, which is called as symmetric structure. It can enhance evanescent waves to achieve super-resolution by existing Surface Plasmon Wave (SPW) on the two interfaces of metal/medium. SPW are collective electron oscillations that are coupled with electromagnetic waves at the interface between dielectrics and metal [11, 12], and different surface plasmons [13–18] (SPs) modes can affect on imaging resolution of metallic superlens [19]. However, many theories and experiments [20–22] demonstrate that the intrinsic losses of metallic superlens can cause quite low transmittance through a metal film, which limits their operating range to wavelengths in the vicinity of the plasma frequency and leads to the low image contrast and the low resolution. To overcome these problems, an Anti-Reflection and Phase Control coatings superlens (ARPC-superlens) model is presented in our previous work [23]. ARPC-superlens is composed of a metal slab and two finite thickness dielectric media with different permittivities ε_2 and ε_4, which is called as the finite thickness asymmetric structure. From the point of view of many reports [5–8], only the symmetric structure (SS) of metallic superlens can excite SPW. By using waveguide method, in the Ref. [12] it is first evidenced that the asymmetric structure (AS) can also excite SPW. However, because these dielectric media are assumed as semi-infinite, and the reflected wave on dielectric media surface has not been considered, the results are not accurate enough, especially for ARPC-superlens. So the performance of SPs modes of finite thickness asymmetric structure has been unclear.

In this manuscript, SPs modes of ARPC-superlens asymmetric structure are firstly discussed based on electromagnetic theory and it is found that there are two asymmetric SPs modes defined as Up Asymmetric Mode and Down Asymmetric Mode. In order to further confirm NIM characteristics of ARPC-superlens, the group velocity of different modes have been compared, which denotes NIM characteristics when the energy flow is anti-parallel to the wave vector [2, 20]. The paper discusses in detail the performance of SPs modes and the relation of the SPs modes and the imaging resolution of ARPC-superlens, and explain the reason why the image resolution can be significantly enhanced by ARPC-superlens. Utilizing the numerical analysis, we find that the resolution for Down Asymmetric Mode is higher than that for other SPs modes. Simultaneously, the image quality depending on the metal slab and the ARPC coatings thickness is investigated and the optimal thickness ratio is concluded. All these research results indicate that the super-resolution can be remarkably improved by utilizing anti-symmetric modes.

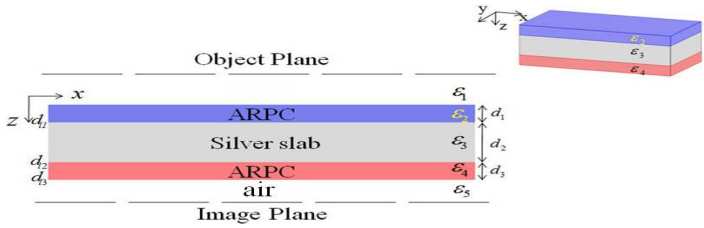

Figure 1. The ARPC-superlens sample structure.

2. SPW DISPERSION RELATION AND WORK MODES ANALYSES

The proposed ARPC-superlens model is made of a superlens and two thin films [23], as shown in Fig. 1. In vacuum, our model is located in x-z plane between $z = 0$ and $z = d_{l3}$; the thickness of two ARPC films and Ag slab are d_1, d_3 and d_2, respectively. The normal wave vector is along z-axis.

The electric field in the slab can be expressed as [23–25]:

$$E_3 = \int_{-\infty}^{\infty} dk_x e^{ik_3 x}\left(B_1 e^{ik_3 z} - B_2 e^{-ik_3 z}\right)/D$$

where

$$B_1 = \left(1 + \frac{k_4\varepsilon_3}{k_3\varepsilon_4} + \frac{k_1\varepsilon_4}{k_4\varepsilon_1} + \frac{k_1\varepsilon_3}{k_3\varepsilon_1}\right) e^{i\left(k_z^{(4)}d_2 - k_3 d_2 + k_1 d_3 - k_z^{(4)} d_3\right)}$$
$$+ \left(1 - \frac{k_4\varepsilon_3}{k_3\varepsilon_4} - \frac{k_1\varepsilon_4}{k_4\varepsilon_1} + \frac{k_1\varepsilon_3}{k_3\varepsilon_1}\right) e^{i(-k_4 d_2 - k_3 d_2 + k_1 d_3 + k_4 d_3)}$$

$$B_2 = \left(1 - \frac{k_4\varepsilon_3}{k_3\varepsilon_4} + \frac{k_1\varepsilon_4}{k_4\varepsilon_1} - \frac{k_1\varepsilon_3}{k_3\varepsilon_1}\right) e^{i(k_4 d_2 + k_3 d_2 + k_1 d_3 - k_4 d_3)}$$
$$+ \left(1 + \frac{k_4\varepsilon_3}{k_1\varepsilon_4} - \frac{k_1\varepsilon_4}{k_4\varepsilon_1} - \frac{k_1\varepsilon_3}{k_3\varepsilon_1}\right) e^{i(-k_4 d_2 + k_3 d_2 + k_1 d_3 + k_4 d_3)}$$

$$D = H_1 + H_2 + H_3 + H_4 + H_5 + H_6 + H_7 + H_8$$

$$H_1 = (1 - k_2/(k_1\varepsilon_2))(1 + k_3\varepsilon_2/(k_2\varepsilon_3))(1 - k_4\varepsilon_3/(k_3\varepsilon_4))(1 + k_1\varepsilon_4/(k_4))\, e^{\vartheta_1};$$

$$H_2 = (1 + k_2/(k_1\varepsilon_2))(1 - k_3\varepsilon_2/(k_2\varepsilon_3))(1 - k_4\varepsilon_3/(k_3\varepsilon_4))(1 + k_1\varepsilon_4/(k_4))\, e^{\vartheta_2};$$

$$H_3 = (1 - k_2/(k_1\varepsilon_2))\,(1 - k_3\varepsilon_2/(k_2\varepsilon_3))(1 + k_4\varepsilon_3/(k_3\varepsilon_4))(1 - k_1\varepsilon_4/(k_4))\, e^{\vartheta_3};$$

$$H_4 = (1 + k_2/(k_1\varepsilon_2))(1 - k_3\varepsilon_2/(k_2\varepsilon_3))(1 + k_4\varepsilon_3/(k_3\varepsilon_4))(1 - k_1\varepsilon_4/(k_4))\, e^{\vartheta_4};$$

$$H_5=(1-k_2/(k_1\varepsilon_2))(1-k_3\varepsilon_2/(k_2\varepsilon_3))(1-k_4\varepsilon_3/(k_3\varepsilon_4))(1-k_1\varepsilon_4/(k_4))\,e^{\vartheta_5};$$
$$H_6=(1+k_2/(k_1\varepsilon_2))(1+k_3\varepsilon_2/(k_2\varepsilon_3))(1-k_4\varepsilon_3/(k_3\varepsilon_4))(1-k_1\varepsilon_4/(k_4))\,e^{\vartheta_6};$$
$$H_7=(1-k_2/(k_1\varepsilon_2))(1-k_3\varepsilon_2/(k_2\varepsilon_3))(1+k_4\varepsilon_3/(k_3\varepsilon_4))(1+k_1\varepsilon_4/(k_4))\,e^{\vartheta_7};$$
$$H_8=(1+k_2/(k_1\varepsilon_2))(1+k_3\varepsilon_2/(k_2\varepsilon_3))(1+k_4\varepsilon_3/(k_3\varepsilon_4))(1+k_1\varepsilon_4/(k_4))\,e^{\vartheta_8};$$
$$\vartheta_1=[ik_3\,(d_1-d_2)-(ik_4\,(d_3-d_2)+ik_2d_1)]+ik_1d_{l3};$$
$$\vartheta_2=[ik_3\,(d_1-d_2)+(ik_4\,(d_3-d_2)-ik_2d_1)]+ik_1d_3;$$
$$\vartheta_3=[-ik_3\,(d_1-d_2)-(ik_4\,(d_3-d_2)+ik_2d_1)]+ik_1d_3;$$
$$\vartheta_4=[-ik_3\,(d_1-d_2)+(ik_4\,(d_3-d_2)-ik_2d_1)]+ik_1d_3;$$
$$\vartheta_5=-[-ik_3\,(d_1-d_2)+(ik_4\,(d_3-d_2)-ik_2d_1)]+ik_1d_3;$$
$$\vartheta_6=-[-ik_3\,(d_1-d_2)-(ik_4\,(d_3-d_2)+ik_2d_1)]+ik_1d_3;$$
$$\vartheta_7=-[ik_3\,(d_1-d_2)+(ik_4\,(d_3-d_2)-ik_2d_1)]+ik_1d_3;$$
$$\vartheta_8=-[ik_3\,(d_1-d_2)-(ik_4\,(d_3-d_2)+ik_2d_1)]+ik_1d_l;$$

Physically, the poles of the integrand in the electric field expression E_3 correspond to the propagation constants of the guided modes. Thus the mode solutions can be easily obtained by letting $D=0$ and inspecting the distributions of zeros [24]. So we can get the dispersion relation [12] of

$$\begin{aligned}k_3\varepsilon_2=&-k_2(4k_1^2\varepsilon_3k_3\varepsilon_4^2Q_6+k_3k_4\varepsilon_3k_1\varepsilon_4e^{ik_1(d_1+d_2+d_3)}Q_1\\&+k_3^2\varepsilon_4^2k_1e^{ik_1(d_1+d_2+d_3)}Q_2+2k_1^2\varepsilon_3^2\varepsilon_4k_4e^{ik_1(d_1+d_2+d_3)}Q_3\\&+4k_1\varepsilon_3^2k_4^2(\cos(\varphi_1')-\cos(\varphi_2')+8k_1\varepsilon_3k_3\varepsilon_4k_4)/k_1\big(4k_3\varepsilon_4k_4\big(\cos(\vartheta_1')\\&+\cos(\vartheta_2')\big)+k_1k_3\varepsilon_4^2e^{ik_1(d_1+d_2+d_3)}Q_4+k_1k_4\varepsilon_3\varepsilon_4e^{ik_1(d_1+d_2+d_3)}Q_5\\&+2k_4^2\varepsilon_3(-\cos(\vartheta_1)+\cos(\vartheta_2)-\cos(\vartheta_3)+\cos(\vartheta_4))\big)\end{aligned}\tag{1}$$

or,

$$\begin{aligned}k_3\varepsilon_4=&-k_2\Big(k_3k_4\varepsilon_3k_1\varepsilon_2e^{ik_1(d_1+d_2+d_3)}W_1+2k_1^2\varepsilon_3^2k_4\varepsilon_2e^{ik_1(d_1+d_2+d_3)}W_2\\&+4k_1^2\varepsilon_3k_3\varepsilon_2^2W_3+k_3^2\varepsilon_2^2k_1e^{ik_1(d_1+d_2+d_3)}W_4+4k_1\varepsilon_3^2k_4^2\left(\cos(\varphi_1')\right.\\&\left.-\cos(\varphi_2')\right)+8k_1\varepsilon_3k_3\varepsilon_2k_4\Big)/k_1(-4k_3\varepsilon_2k_4(\cos(\vartheta_2')+\cos(\vartheta_1'))\\&-k_1k_4\varepsilon_3\varepsilon_2e^{(k_1d_1+k_1d_2+k_1d_3)}W_5+k_1k_3\varepsilon_2^2e^{ik_1(d_1+d_2+d_3)}W_6\\&+2k_4^2\varepsilon_3(\cos(\vartheta_4)-\cos(\vartheta_1)+\cos(\vartheta_2)-\cos(\vartheta_3)))\end{aligned}\tag{2}$$

where,

$$\begin{aligned}Q_1&=(e_1+e_2+e_3+e_4+e_5+e_6+e_7+e_8);\\Q_2&=(-e_{11}+e_{22}-e_{33}+e_{44}+e_{55}-e_{66}+e_{77}-e_{88});\end{aligned}$$

$$
\begin{aligned}
Q_3 &= (ex_1 + ex_2 - ex_3 - ex_4);\\
Q_4 &= (-e_{11} - e_{22} - e_{33} - e_{44} + e_{55} + e_{66} + e_{77} + e_{88});\\
Q_5 &= (e_1 + e_2 + e_3 + e_4 - e_5 - e_6 - e_7 - e_8);\\
Q_6 &= \left(e^{(i(k_1-k_4)(d_1+d_2+d_3))} - e_2^{(i(k_1+k_4)(d_1+d_2+d_3))}\right);\\
e_1 &= e^{(i(-d_1k_2+k_3d_2+k_4d_3))}; \quad e_2 = e^{(i(-d_1k_2-k_3d_2+k_4d_3))};\\
e_3 &= e^{(i(d_1k_2+k_3d_2+k_4d_3))}; \quad e_4 = e^{(i(d_1k_2-k_3d_2+k_4d_3))};\\
e_5 &= e^{(i(-d_1k_2-k_3d_2-k_4d_3))}; \quad e_6 = e^{(i(-d_1k_2+k_3d_2-k_4d_3))};\\
e_7 &= e^{(i(d_1k_2-k_3d_2-k_4d_3))}; \quad e_8 = e^{(i(d_1k_2+k_3d_2-k_4d_3))};\\
e_{11} &= e^{(i(-d_1k_3+d_1k_2-k_4d_1-k_4d_2-k_4d_3))};\\
e_{22} &= e^{(i(-d_1k_3-d_1k_2+k_4d_1+k_4d_2+k_4d_3))};\\
e_{33} &= e^{(i(-d_1k_3-d_1k_2-k_4d_1-k_4d_2-k_4d_3))};\\
e_{44} &= e^{(i(d_1k_3+d_1k_2-k_4d_1-k_4d_2-k_4d_3))};\\
e_{55} &= e^{(i(-d_1k_3+d_1k_2+k_4d_1+k_4d_2+k_4d_3))};\\
e_{66} &= e^{(i(d_1k_3-d_1k_2+k_4d_1+k_4d_2+k_4d_3))};\\
e_{77} &= e^{(i(d_1k_3-d_1k_2-k_4d_1-k_4d_2-k_4d_3))};\\
e_{88} &= e^{(i(d_1k_3+d_1k_2+k_4d_1+k_4d_2+k_4d_3))};\\
ex_1 &= e^{(i(-d_1k_3-k_3d_2-k_4d_3))}; \quad ex_2 = e^{(i(-d_1k_3-k_3d_2+k_4d_3))};\\
ex_3 &= e^{(i(d_1k_3+k_3d_2+k_4d_3))}; \quad ex_4 = e^{(i(d_1k_3+k_3d_2-k_4d_3))};\\
\phi_1' &= ((-k_4+k_3)(d_1+d_2)); \quad \phi_2' = ((k_4+k_3)(d_1+d_2));\\
\vartheta_1 &= (d_1k_2+k_4d_1+k_4d_2+k_3d_2); \quad \vartheta_2 = (d_1k_2-k_4d_1-k_4d_2+k_3d_2);\\
\vartheta_3 &= (d_1k_2+k_4d_1+k_4d_2+k_3d_2); \quad \vartheta_4 = (d_1k_2-k_4d_1-k_4d_2-k_3d_2);\\
\vartheta_1' &= ((-k_3+k_2)d_1); \quad \vartheta_2' = ((k_3+k_2)d_1);
\end{aligned}
$$

By the above derivation, we note that there are two SPs modes for the asymmetric structure with finite thick dielectric media.

Compared with the dispersion relation of asymmetric structure, the dispersion relation of the symmetric structure ($\varepsilon_2 = \varepsilon_4$) is shown by using the waveguide method [19]:

$$\varepsilon_3 k_2 + \varepsilon_2 k_3 \tanh\left(\frac{ik_1\,(d_2)}{2}\right) = 0 \tag{3}$$

or

$$\varepsilon_3 k_2 + \varepsilon_2 k_3 \coth\left(\frac{ik_1\,(d_2)}{2}\right) = 0 \tag{4}$$

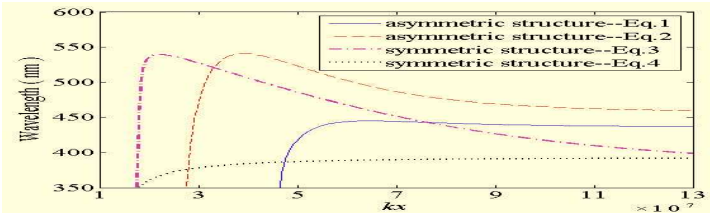

Figure 2. Dispersion curve of surface plasmons for asymmetric and symmetric structure.

3. NUMERICAL SIMULATIONS

The softwares of COMSOL Multiphysics and Matlab are used for simulation. In following figures, the units of x and z are meter. When a metallic film is embedded in dielectric media and the film thickness d is smaller than the penetration depth of SPs, the interaction between the two SPs on the two metal-dielectric interfaces cannot be neglected [11]. The coupled modes are generally called antisymmetric and symmetric plasmon modes in the symmetric structure [26]. Firstly, we discuss the dispersion curve for SPs by using Eqs. (1)–(4). Fig. 2 represents the dispersion relation of SPs at the interface between the silver slab and ARPC, when thickness ratio is 2:1. The Drude model [27] for silver is taken as

$$\varepsilon_3 = \varepsilon_3' + i \cdot \varepsilon_3'' = \left(1 - \omega_p^2 / \left(\omega^2 + i\omega\Gamma\right)\right) \tag{5}$$

where ω_p is the plasma frequency [27], Γ the relaxation constant, and ω the angular frequency of the source. The permittivities ε_2 and ε_4 are 1.2 and 1/1.2, respectively. From Fig. 2, it can be seen that SPs have a larger wave vector. Because the group velocity [28] is defined as $v_g = d\omega/dk$, the antisymmetric mode possesses negative slope at the large wave vector region, indicating that the group velocity is negative [26]. In contrast, the slope of the SPs dispersion curve for the symmetric mode is always positive. So, we can define the Eqs. (1)–(3) as asymmetric modes and the Eq. (4) as symmetric mode.

Now we consider different propagation characteristics of SPs modes with opposite group velocities. A Gaussian beam with a finite waist and TM polarization (magnetic field is along y axis) is incident from up ARPC coating and the incident angle is the intersection angle between the incident wave vector and x-axis. The incident light can resonantly excite the SP mode through the evanescent wave penetrating from the surround media (similar a prism, with a permittivity $\varepsilon_1 = 5.8$) into the up ARPC coating if the tangential component of the wave vector (k_x) is matched to that of the desired

SP mode (k_{SPP}), as following Eq. (6):

$$k_x = \frac{\omega}{c}\sqrt{\frac{\varepsilon_1}{\varepsilon_2}}\sin\theta_{in} = \frac{\omega}{c}\sqrt{\frac{\varepsilon_3'\varepsilon_4}{\varepsilon_3'+\varepsilon_4}} = k_{SPP} \tag{6}$$

So we can obtain that the incident angle is 25.7° according to corresponding ε_3', ε_1, ε_2 and ε_4 by using Eq. (6). The medium 1 play a role a prism. The x-component of the electric field is shown in Fig. 3. The field profiles in Figs. 3(a)–(c) are asymmetric modes and we can see that the surface wave propagates backward, compared with the positive phase velocity in the x-direction. It indicates that the group velocity is antiparallel to the phase velocity under asymmetric modes [26], which is predicted by the negative slope of the dispersion curve in Fig. 2. It is confirmed that in asymmetric modes the metal slab can play a role of NIM because when an electromagnetic plane wave propagates in it, the direction of Poynting vector will be opposite to that of wave-vector (k) so that k, E, H form a left-handed set of vectors [2, 20]. And it is conducive to enhancing evanescent waves to achieve super-resolution image [1]. The symmetric SP mode is shown in Fig. 3(d). In contrast to what one can see in Figs. 3(a)–(c), the field profile in Fig. 3(d) indicates that the surface plasmon propagates forwards; that is, both the group velocity and phase velocity are positive in the x-direction. Moreover, it is unfavorable to achieve super-resolution image.

In order to obtain the optical energy which is transmitted into the asymmetric structure in this case, the reflection coefficient R on the metallic slab can be calculated by considering the resonance of the multiply reflected field within the ARPC-superlens [1]:

$$R = \left|\frac{r_{12} + r^1 e^{(2id_1k_1)}}{1 + r_{12}r^1 e^{(2i\omega d_1 k_1)}}\right|^2 \tag{7}$$

where $k_i = \sqrt{\varepsilon_i - \varepsilon_1 \sin^2\theta_1} \times \omega/c$, $i = 1, 2, 3, 4, 5$, $r_{ij} = (\sqrt{\varepsilon_j}\cos\theta_i - \sqrt{\varepsilon_i}\cos\theta_j)/(\sqrt{\varepsilon_j}\cos\theta_i + \sqrt{\varepsilon_i}\cos\theta_j)$, θ_i is incident angle and θ_j is the refractive angle in i layer, $r^1 = r_{23} + r^2 e^{(2id_2k_2)}/1 + r_{23}r^2 e^{(2id_2k_2)}$, $r^2 = r_{34} + r_{41}e^{(2id_3k_3)}/1 + r_{34}r_{41}e^{(2id_3k_3)}$. And Fig. 4 shows the reflection coefficient R as a function of the incident angle. Only incident angle is 25.7°, the value of R can be the minimum, which means that SPW has been excited and the most optical energy is coupled with SPW. As the metal film thickness decreases the SP mode splits into the two modes designated the long-range surface Plasmon (LRSP) and the short-range surface Plasmon (SRSP) such that the real part of the wave vector for the LRSP mode decreases and that of the SRSP increases. Further, the imaginary part of the mode wave

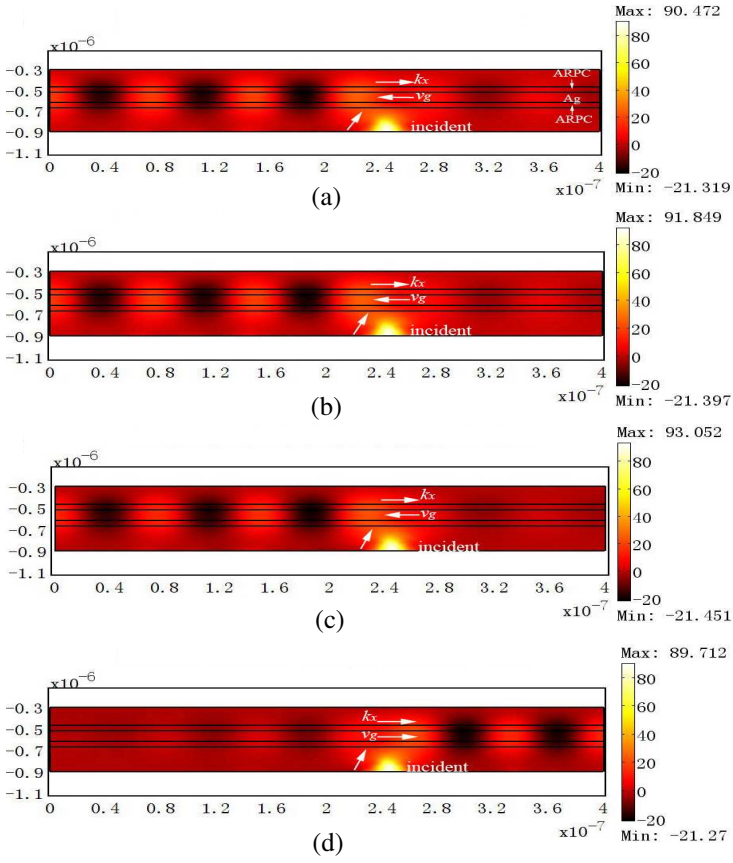

Figure 3. Field profile of backward and forward propagating surface plasmons ($\varepsilon_1 = 5.8$): (a) Asymmetric mode of Eq. (1) ($\lambda = 447$ nm, $\varepsilon_2 = 1.6$, $\varepsilon_4 = 1/1.6$); (b) Asymmetric mode of Eq. (2) ($\lambda = 490$ nm, $\varepsilon_2 = 1.2$, $\varepsilon_4 = 1/1.2$); (c) Asymmetric mode of Eq. (3) ($\lambda = 457$ nm, $\varepsilon_2 = \varepsilon_4 = 1.48$); (d) Symmetric mode of Eq. (4) ($\lambda = 396$ nm, $\varepsilon_2 = \varepsilon_4 = 1.9$).

vector of the LRSP decreases relative to that of the SRSP, producing a narrowing of the LRSP resonance curve [29]. These features are seen in Fig. 4, where we can get the conclusion that LRSP can be excited in the asymmetric structure.

In the following, Figs. 5(a)–(d) show the magnetic field intensity distribution of the ARPC-superlens with different SPs modes. The simulation domain consists of a mask with the double slits of 20 nm slit width, 25 nm ARPC coatings and a 50 nm silver film, and the

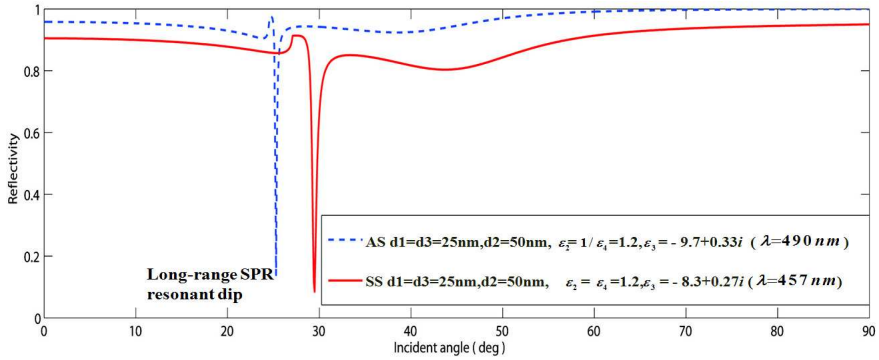

Figure 4. The reflection coefficient R as a function of the incident angle ($\varepsilon_1 = 5.8$).

incident angle can be got by using Eq. (7). All the permittivities ε_i are equivalent to those of Fig. 3. Fig. 5(a) is obtained by using Eq. (1) and it is obvious that the magnetic field strength on the upper ARPC coating is the strongest, so it is called Up Asymmetric Mode (UAM). Fig. 5(b) is obtained by using Eq. (2) and it is obvious that the magnetic field strength on the lower ARPC coating is the strongest, so it is called Down Asymmetric Mode (DAM). Fig. 5(c) is obtained by using Eq. (3) and it is obvious that the magnetic field strength remains the strongest on two ARPC coatings, so it is called Even Asymmetric Mode. Fig. 5(d) is obtained by using Eq. (4) and it is obvious that the magnetic field strength on the silver slab is the strongest, so it is called Symmetric Mode. The different modes have different propagation characteristics and different magnetic field intensity distributions, which are shown in Figs. 3–5. The Up Asymmetric Mode is confined to the upper interface while the Down Asymmetric Mode is confined to the lower interface. So their reflection coefficients R are different, which are shown in Fig. 6.

From Fig. 6, Up Asymmetric Mode and Down Asymmetric Mode are equivalent to LRSP when both the thicknesses of ARPC coating and metal slab are thinner and the metal/ARPC thickness ratio is 2:1. In contrast to what one can see in Fig. 6, Up Asymmetric Mode and Down Asymmetric Mode are equivalent to SRSP when both the thicknesses of ARPC coating and metal slab are thicker and the metal/ARPC thickness ratio is 1:1. This negative reflection peak provides SPP amplification, which is necessary to compensate for its exponential decay along the z axis [12]. So the imaging resolution of LRSP should be higher than that of SRSP. This means that image

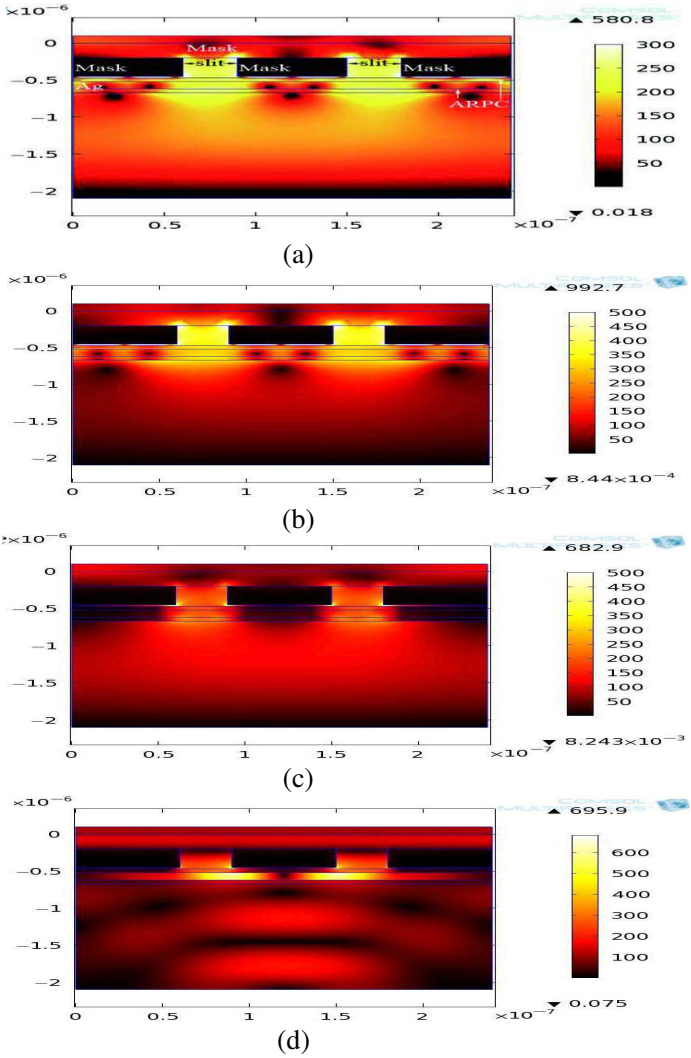

Figure 5. The magnetic field intensity distribution of the ARPC-superlens with different SPs modes: (a) Up asymmetric mode; (b) Down asymmetric mode; (c) Even asymmetric mode; (d) Symmetric mode.

resolution can be greatly improved when the metal/ARPC thickness ratio is 2:1.

In order to get the relation of the imaging resolution of ARPC-superlens and SPs modes, we discussed the lateral intensity

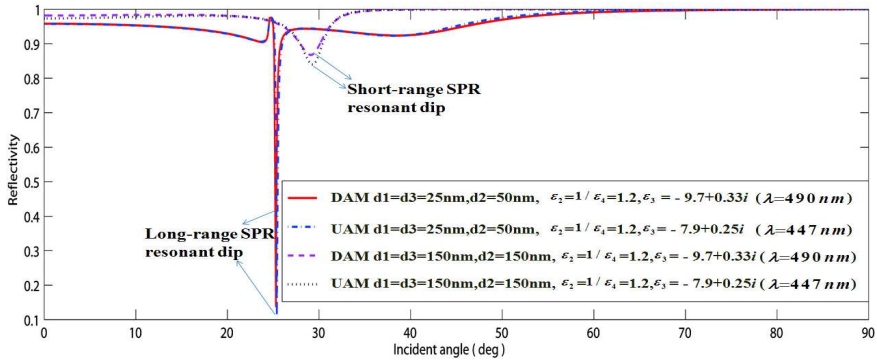

Figure 6. The reflection coefficient R as a function of the incident angle for up asymmetric mode and down asymmetric mode ($\varepsilon_1 = 5.8$).

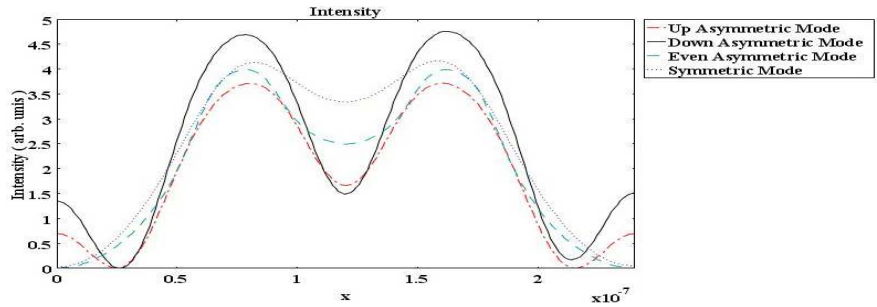

Figure 7. The lateral intensity distributions through 20 nm width double slit. The dash-dot line the solid line, the dash line and the dot line represents the up asymmetric mode ($\lambda = 447$ nm, $\varepsilon_2 = 1.6$, $\varepsilon_4 = 1/1.6$), down asymmetric mode ($\lambda = 490$ nm, $\varepsilon_2 = 1.25$, $\varepsilon_4 = 1/1.2$), even asymmetric mode ($\lambda = 457$ nm, $\varepsilon_2 = \varepsilon_4 = 1.48$), symmetric mode ($\lambda = 396nm$, $\varepsilon_2 = \varepsilon_4 = 1.9$), respectively, when the sliver slab thickness is 50 nm and ARPC coating thickness is 25 nm.

distributions through the double slits of 20 nm slit width, as shown in Fig. 7. Whether the double-slit can be distinguished in the image plane is dependent on the minimum value of intensity at the central location. So, it is obvious that the imaging resolution under Up Asymmetric Mode and Down Asymmetric Mode are higher than that under Even Asymmetric Mode and Symmetric Mode. And by using the image contrast formula,

$$C = \frac{I_{\max} - I_{\min}}{I_{\max} + I_{\min}} \tag{8}$$

we can obtain the image contrast shown in Table 1. So the image contrast can be greatly improved by Down Asymmetric Mode and Up Asymmetric Mode. The reason is that intrinsic loss of absorption in the Ag slab superlens turn out to add a blurring effect to the ideal image reconstruction for the impedance match case [22], but the magnetic field of Down Asymmetric Mode or Up Asymmetric Mode can be concentrated on the two ARPC coatings, which can reduce the intrinsic loss of absorption in the Ag slab. So the image contrast can be improved for the impedance mismatch case. It reconfirms that the ARPC-superlens can significantly enhance the image contrast and resolving capability under the constraint relations [23].

Physically, because of large k_x, the penetration depth of SPs into the metal is small compared with the film thickness, and therefore SPs at each interface are decoupled. For this reason, we study the lateral intensity distributions to get the optimal ratio between the metal slab and the ARPC coatings thickness, as shown in Fig. 8. The Down Asymmetric Mode and Up Asymmetric Mode are shown in Figs. 8(a) and (b), respectively. We can see that the imaging resolution is higher when the metal/ARPC thickness ratio is 2:1 under the asymmetric structure. By using the image contrast formula Eq. (6) to further measure the imaging quality, as shown in Table 2, we can obtain the image contrast which is greatly improved by Down Asymmetric Mode

Table 1. The image contrast with different SPs modes.

SPs Modes	Up Asymmetric Mode	Down Asymmetric Mode	Even Asymmetric Mode	Symmetric Mode
Image Contrast	0.38	0.52	0.14	0.08

Table 2. The image contrast with different SPs modes and thickness ratio.

Metal/ARPC thickness ratio (Ag/ARPC (nm))	2:1 (50/25)	2:1 (40/20)	4:1 (40/10)	1:1 (50/50)	1:1 (40/40)	3:2 (60/40)	1:2 (25/50)
Down Asymmetric Mode	0.52	0.48	0.43	0.25	0.18	0.16	0.07
Up Asymmetric Mode	0.38	0.21	0.2	0.19	0.15	0.18	0.08

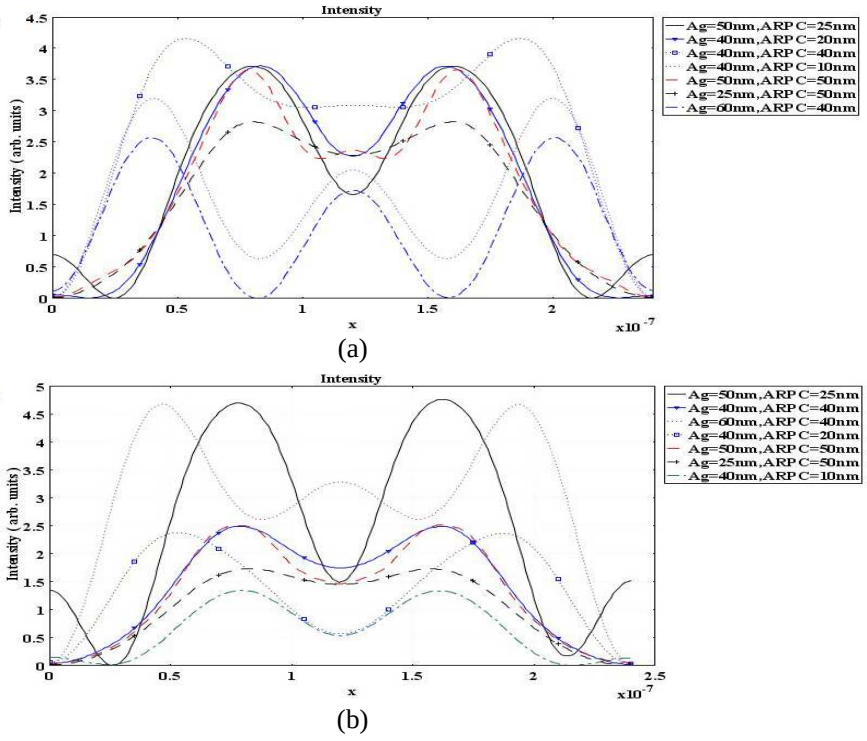

Figure 8. The lateral intensity distributions through 20 nm width double slit: (a) Down asymmetric mode; (b) Up asymmetric mode.

when the metal/ARPC thickness ratio is 2:1. These results confirm the conclusion of Fig. 6.

4. CONCLUSION

In this paper, we discuss SPs modes of finite thickness asymmetric structure and obtain two asymmetric SPs modes with ARPC-superlens asymmetric structure, which are named Up Asymmetric Mode and Down Asymmetric Mode. These modes can be excited by using a high refractive index medium up the upper ARPC coating. The purpose of this medium is to increase the wave vector of the incident light so that its component along the interface can match the wave vector of the SPP at the metal-dielectric interface. Because the magnetic field of these asymmetric modes can be concentrated on the two ARPC coatings, which can reduce the intrinsic loss of absorption in the Ag slab, the image resolution can be significantly enhanced by

ARPC-superlens. Simultaneously, the optimal ratio between the metal slab and the ARPC coatings thickness is concluded. The numerical analysis indicates that the image contrast and resolving capability can be significantly enhanced under the Down Asymmetric Mode when the metal/ARPC thickness ratio is 2:1. These conclusions reconfirm that the ARPC-superlens can greatly improve the image contrast and resolving capability under the matching conditions and constraint relations. This ARPC-superlens with asymmetric modes is believed to be applicable to optical nanoimaging, bio-sensoring and lithography.

ACKNOWLEDGMENT

This work was supported by the Fundamental Research Funds for the Central Universities (lzujbky-2011-k02).

REFERENCES

1. Pendry, J. B., "Negative refraction makes a perfect lens," *Phys. Rev. Lett.*, Vol. 85, 3966, 2000.
2. Veselago, V. G., "Properties of materials having simultaneously negative values of dielectric (ε) and magnetic (μ) susceptibilities," *Sov. Phys. Solid State*, Vol. 8, 2854–2856, 1967.
3. Zhang, Y., T. M. Grzegorczyk, and J. A. Kong, "Propagation of electromagnetic waves in a slab with negative permittivity and negative permeability," *Progress In Electromagnetics Research*, Vol. 35, 271–286, 2002.
4. Mahmoud, S. F. and A. J. Viitanen, "Surface wave character on a slab of metamaterial with negative permittivity and permeability," *Progress In Electromagnetics Research*, Vol. 51, 127–137, 2005.
5. Liu, Z. W., N. Fang, T.-J. Yen, and X. Zhang, "Rapid growth of evanescent wave by a silver superlens," *Appl. Phys. Lett.*, Vol. 83, 5184, 2003.
6. Moore, C. P., M. D. Arnold, P. J. Bones, and R. J. Blaikie, "Image fidelity for single-layer and multi-layer silver superlenses," *JOSA A*, Vol. 25, No. 4, 911–918, 2008.
7. Shi, Z., V. Kochergin, and F. Wang, "193 nm superlens imaging structure for 20 nm lithography node," *Optics Express*, Vol. 17, No. 14, 11309–11314, 2009.
8. Chaturvedi, P., W. Wu, V. J. Logeeswaran, Z. Yu, M. S. Islam, S. Y. Wang, R. S. Williams, and N. X. Fang, "A smooth optical superlens," *Appl. Phys. Lett.*, Vol. 96, 043102, 2010.

9. Chuang, C.-H. and Y.-L. Lo, "Signal analysis of aperture less scanning near-field optical microscopy with superlens," *Progress In Electromagnetics Research*, Vol. 109, 83–106, 2010.
10. Jin, Y., "Improving subwavelength resolution of multilayered structures containing negative-permittivity layers by flatting the transmission curves," *Progress In Electromagnetics Research*, Vol. 105, 347–364, 2010.
11. Raether, H., *Surface Plasmons*, Springer, Berlin, 1988.
12. Tremblay, G. and Y. Sheng, "Improving imaging performance of a metallic superlens using the long-range surface plasmon polariton mode cutoff technique," *Applied Optics*, Vol. 49, No. 7, 1, 2010.
13. Chau, Y. F., H. H. Yeh, and D. P. Tsai, "Surface plasmon resonances effects on different patterns of solid-silver and silver-shell nanocylindrical pairs," *Journal of Electromagnetic Waves and Applications*, Vol. 24, No. 8–9, 1005–1014, 2010.
14. Suyama, T., Y. Okuno, and T. Matsuda, "Surface plasmon resonance absorption in a multilayered thin-film grating," *Journal of Electromagnetic Waves and Applications*, Vol. 23, No. 13, 1773–1783, 2009.
15. Li, Y. and X. Zhang, "Nonlinear optical switch utilizing long-range surface plasmon polaritons," *Journal of Electromagnetic Waves and Applications*, Vol. 23, No. 17–18, 2363–2371, 2009.
16. Xie, H., F. Kong, and K. Li, "The electric field enhancement and resonance in optical antenna composed of Au nanoparicles," *Journal of Electromagnetic Waves and Applications*, Vol. 23, No. 4, 535–548, 2009.
17. X. Li, Y. Ye, and Y. Jin, "Impedance-mismatched hyperlens with increasing layer thicknesses," *Progress In Electromagnetics Research*, Vol. 118, 273–286, 2011.
18. J. Zhao, K. Li, F. Kong, and D. Liu-Ge, "Enhancement of blue light emission using surface plasmons coupling with quantum wells," *Progress In Electromagnetics Research*, Vol. 108, 293–306, 2010.
19. Xu, T., L. Fang, J. Ma, B. Zeng, Y. Liu, J. Cui, C. Wang, Q. Feng, and X. Luo, "Localizing surface plasmons with a metal-cladding superlens for projecting deep-subwavelength patterns," *Appl. Phys. B*, Vol. 97, No. 1, 175–179, 2009.
20. Cao, P., X. Zhang, L. Cheng, and Q. Meng, "Far field imaging research based on multilayer positive- and negative-refractive-index media under off-axis illumination," *Progress In Electromagnetics Research*, Vol. 98, 283–298, 2009.

21. Lee, K., Y. Jung, G. Kang, H. Park, and K. Kim, "Active phase control of a Ag near-field superlens via the index mismatch approach," *Appl. Phys. Lett.*, Vol. 94, 101113, 2009.
22. Lee, K., H. Park, J. Kim, G. Kang, and K. Kim, "Improved image quality of a Ag slab near-field superlens with intrinsic loss of absorption," *Optics Express*, Vol. 16, No. 3, 1711–1718, 2008.
23. Cao, P., L. Cheng, Y. E. Li, X. Zhang, Q. Meng, and W. J. Kong, "Reflectivity and phase control research for superresolution enhancement via the thin films mismatch," *Progress In Electromagnetics Research*, Vol. 107, 365–378, 2010.
24. Cheng, Q. and T. J. Cui, "Guided modes in a planar anisotropic biaxial slab with partially negative permittivity and permeability," *Appl. Phy. Lett.*, Vol. 87, No. 17, 174102, 2005.
25. Ye, Z., "Optical transmission and reflection of perfect lenses by left handed materials," *Phys. Rev. B*, Vol. 67, 193106, 2003.
26. Liu, Y., D. F. P. Pile, Z. Liu, D. Wu, C. Sun, and X. Zhang, "Negative group velocity of surface plasmons on thin metallic films," *Proc. SPIE*, Vol. 6323, 63231M, 2006.
27. Fox, M., *Optical Properties of Solids*, Oxford Univerity Press, 2001.
28. Monti, G. and L. Tarricone, "Negative group velocity in a split ring resonator-coupled microstrip line," *Progress In Electromagnetics Research*, Vol. 94, 33–47, 2009.
29. Chen, Z. and H. J. Simon, "Attenuated total reflectance from a layered silver grating with coupled surface waves," *JOSA B*, 5, 1988.